Journal of Advanced Research 28 (2021) 221–229

Contents lists available at ScienceDirect

Journal of Advanced Research

journal homepage: www.elsevier.com/locate/jare

A novel experimental approach to evaluate guided bone regeneration (GBR) in the rat femur using a 3D-printed CAD/CAM zirconia space-maintaining barrier

Alexandru Petre [a], Cornel Balta [b], Hildegard Herman [b], Sami Gharbia [b,e], Ada Codreanu [c], Bianca Onita-Mladin [b], Nicoleta Anghel-Zurbau [c], Andrei-Gelu Hermenean [d], Simona-Rebeca Ignat [e], Sorina Dinescu [e], Iuliana Urzica [f], Sergiu Drafta [a], Luminita Oancea [a], Anca Hermenean [b,c,e,*]

[a] *Occlusion and Fixed Prosthodontic Department, Carol Davila University of Medicine and Pharmacy, Bucharest, Romania*
[b] *"Aurel Ardelean" Institute of Life Sciences, Vasile Goldis Western University of Arad, Romania*
[c] *Department of Histology, Faculty of Medicine, Vasile Goldis Western University of Arad, Romania*
[d] *Faculty of Medicine, Carol Davila University of Medicine and Pharmacy, Bucharest, Romania*
[e] *Department of Biochemistry and Molecular Biology, University of Bucharest, Romania*
[f] *National Institute for Lasers, Plasma and Radiation Physics, Lasers Department, Bucharest, Romania*

GRAPHICAL ABSTRACT

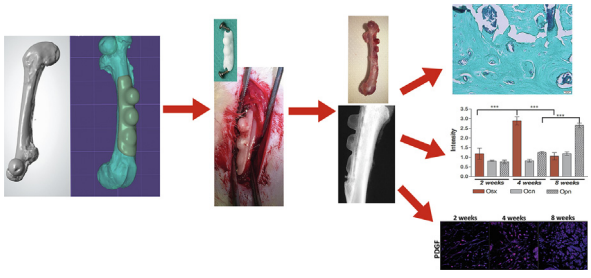

ARTICLE INFO

Article history:
Received 31 March 2020
Revised 20 July 2020
Accepted 20 July 2020
Available online 23 July 2020

Keywords:
Bioengineering
Bone remodeling
Bone regeneration
Guided tissue regeneration
Zirconia

ABSTRACT

Introduction: Obtaining a certain bone volume is an important goal in implantology or orthopedics. Thus, after tooth extraction, quite a lot of horizontal and vertical alveolar bone is lost in time and can be detrimental to the implant treatment outcome, while the treatment of critical bone defects is a considerable challenge for surgery.
Objectives: In this study we designed a new in vivo model as an useful experimental tool to assess guided bone regeneration (GBR) using a computer-aided design/manufacturing (CAD-CAM) space-maintaining barrier.
Methods: The barrier was 3D printed with three progressive heights, surgically placed on rat femur, and GBR results were analyzed at 2, 4, and 8 weeks by X-ray and bone mineral density analysis, histology/morphometry and by immunofluorescence and immunohistochemistry for osteogenesis and angiogenesis evaluation.

Abbreviations: CAD/CAM, computer-aided design/computer-aided manufacturing; DAPI, 4′,6-diamidino-2-phenylindole; ePTFE, expanded polytetrafluoroethylene; FBS, fetal bovine serum; GAPDH, glyceraldehyde 3-phosphate dehydrogenase; GBR, guided bone regeneration; IVC, individually ventilated cage; PBS, phosphate-buffered saline; PCL, poly(e-caprolactone); PDGFRβ, platelet-derived growth factor receptor β; PFA, paraformaldehyde; PGA, poly(glycolic acid); PLA, poly(lactic acid); OCN, osteocalcin; OPN, osteopontin; OSX, osterix; VEGF, vascular endothelial growth factor; VEGFR, vascular endothelial growth factor receptor.

Peer review under responsibility of Cairo University.

* Corresponding author at: "Aurel Ardelean" Institute of Life Sciences, Vasile Goldis Western University of Arad, 310046, Romania.
E-mail address: anca.hermenean@gmail.com (A. Hermenean).

https://doi.org/10.1016/j.jare.2020.07.012
2090-1232/

Dentistry
Orthodontics

Results: The obtained results show that the proposed experimental model provides a real-time useful information on progressive bone tissue formation, which depends on the volume of isolated space created for GBR and on molecular events that lead to satisfactory vertical and horizontal bone augmentation and osteointegration.
Conclusion: In conclusion, the proposed customized three-dome space-maintaining barrier is suitable as an experimental tool to assess the potential of using the designed barriers in dentistry and orthopedics to promote the formation of new bone and determine their space- and time-dependent limitations. Meanwhile, guided bone augmentation for dentistry requires subsequent evaluation on an alveolar bone preclinical model followed by clinical implementation.

Introduction

Obtaining a certain bone volume is an important goal in implantology or orthopedics. After tooth extraction, the alveolar bone begins to change during the first 3 months [1], loses 2 mm in vertical size and 50% of its horizontal size within 6 months [2,3], and loses up to 60% in the first 3 years [4,5]. Horizontal and vertical alveolar bone deficiencies are detrimental to the final treatment outcome [2,6] and should be corrected before surgical positioning of the implant. Moreover, in orthopedy, the treatment of critical bone defects (e.g., segmental or large cortical defects created by trauma, tumor resection, infection, or *peri*-implant bone loss) is a considerable challenge for surgery [7].

Bone can be augmented by osteogenesis distraction (surgical induction of a fracture), osteoinduction (growth factors, osteoprogenitor cells) and by guided bone regeneration (GBR), which provide isolated spaces between the existing bone and surrounding soft tissues. This objective can be accomplished using space maintainers (e.g., autogenous bone blocks or various types of scaffolds), which are usually covered by barrier membranes that are subsequently filled with newly produced bone [8]. The most important requirement of GBR is the creation of physical barriers to isolate bone defects from the surrounding soft tissue and protect blood clots, which provides osteogenic cells and excludes other cells that restrict osteogenesis (e.g., epithelial cells and fibroblasts) [8,9].

Many bio-resorbable or non-resorbable membranes have been introduced for pre-clinical and clinical evaluation to be used further in GBR medical applications. Bio-resorbable membranes consist of several natural polymers, such as collagen, EMC components, chitosan, alginate, inorganic compounds (calcium sulfate, calcium phosphate hydroxyapatite), or aliphatic polyesters (e.g., PLA, PGA, and PCL). These membranes are considered to be user-friendly, biocompatible, wound healing, and bone formation promoting. Some disadvantages have also been highlighted, such as excessively rapid degradation in vivo and failure to maintain structural integrity, which is necessary for bone regeneration (e.g., collagen) [10], uncontrolled duration of barrier function, undesirable resorption processes [11], or host-tissue response and foreign body reactions during degradation (synthetic membranes) [12,13]. Non-resorbable membranes, such as synthetic polymers [expanded polytetrafluoroethylene (e-PTFE)] and metals (e.g., titanium, titanium alloys, and cobalt–chromium alloys), have been extensively studied [14,15]. These membranes possess the advantages of good biocompatibility, ability to maintain their structural integrity during implantation, and improved space-maintaining properties; thus, these membranes are better than resorbable membranes; however, possible cytotoxic reactions may reduce cellular adhesion [7].

The design of guided tissue regeneration areas can be done intraoperatively based on the surgeon's clinical experience; alternatively, the process can be made more predictable by anatomical reconstructions performed prior to surgery via diagnostic imaging, computerized tomography, or nuclear magnetic resonance [16]. Customized grafts of allogeneic, xenogeneic, and alloplastic origins have been reported for CAD–CAM and 3D printing applications of the alveolar ridge; however, currently, only few products are commercially available [17]. For example, nine patients with atrophic implantation sites were tested using a CAD–CAM customized titanium mesh to promote guided bone augmentation (especially vertical bone gain), and the implant insertion was possible after 6–8 months [18]. Anderud et al. [19] showed that the placement of zirconia domes on a rabbit calvaria induced new bone formation and osteoconduction within 12 weeks. However, the extent of vertical regeneration by this technique has not been clarified. Moreover, the results of a clinical pilot study in implantology established that individual ceramic sheets can regenerate large bone volumes both vertically and horizontally [20]; however, extension to a larger number of subjects is necessary to confirm this hypothesis. Other studies have shown that customized nanohydroxyapatite-enriched CAD–CAM scaffolds induce a larger volume of new bone [21]. There are some results in the field of GBR with applications in orthopedics, such as the evaluation of guided bone regeneration in the rabbit femur using collagen membranes [22] or the correction of critical size segmental femoral defects in rats using equine bone [23].

Upon accounting for the shortcomings of previous studies, we propose an easy screening technique as a first assessment of new material candidates for GBR barriers in dentistry and orthopedics, which can enable the evaluation of the newly formed bone volume and its mineral density to provide information about the limitations in promoting vertical and horizontal bone addition. We aimed to obtain the barrier model using a CAD–CAM dental application to optimize the anatomic situation on the bone site and improve the in vivo biological behavior of the regeneration procedure. The three-dome customized bioceramic barrier was designed by us to provide real-time information about appropriate responses depending on the volume of space where new bone needs to be generated.

In this study, we aimed to answer two questions. First, we were interested to know whether a customized three-dome CAD–CAM barrier can provide information about appropriate responses that are time- and space-dependent (e.g., colonization during GBR, predictable bone volume generation, adequate soft tissue reactions). Second, we wanted to determine whether this model can be used to obtain information on key mechanistic events in the dynamics of osteogenesis and angiogenesis depending on the space size allocated by the barrier. Furthermore, in addition to histology/histomorphometry, in this study, we used radiographic assessment (e.g., high-resolution X-ray imaging) to evaluate and quantify dynamic changes in the new bone structure. The differentiation of progenitor cells, osteogenesis, and angiogenesis markers were analyzed by immunofluorescence and immunohistochemistry.

Materials and methods

CAD–CAM design

In our experimental model, we used a 3D image of a rat femur obtained through optical scanning using an intraoral scanner (Trios

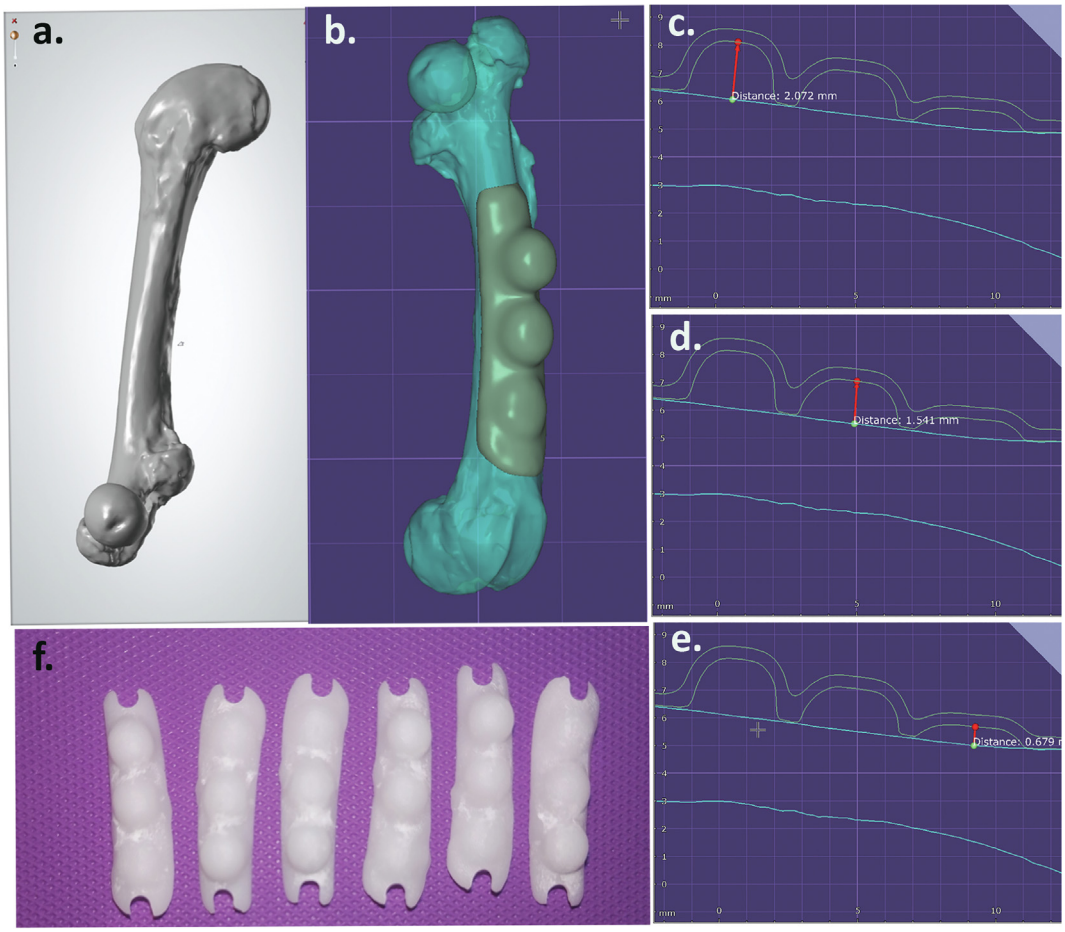

Fig. 1. Design and milling of 3D-customized CAD/CAM zirconia space-maintaining devices. a. 3D image of a rat femur; b. CAD of the membrane; c. Dome with the maximum height design (2.072 mm); d. Dome with the medium height design (1.541 mm); e. Dome with the minimum height design (0.679 mm); f. Printed 3D-customized CAD/CAM zirconia space-maintaining devices before screwing to the rat femurs.

3, 3Shape, Copenhagen, Denmark). The produced 3D file (.stl) was imported into a general dental lab CAD application (Exocad, Exocad Gmbh, Darmstadt, Germany) in which a three-dome customized structure was generated with various heights (Fig. 1).

The size scale of the rat femur corresponds to a sector of the human dental arch of 4–6 cm. For this order of magnitude, dental 3D scanners have demonstrated an accuracy level of several tens of micrometers [24,25].

3D prototyping

The manufacturing of the three-dome customized zirconia membrane was accomplished by milling (Roland 5D, Roland, Japan) using commercially available dental zirconia blanks (Kerox, Kerox Dental, Hungary). The composition is shown in Table 1.

Table 1
Material composition as per manufacturer specification.

Ingredients	Weight percentage
ZrO_2	90.2–94.3%
Y_2O_3	5.7–9.8%
Al_2O_3	<0.25%
SiO_2	<0.02%
Fe_2O_3	<0.02%
Na_2O	<0.02%

The milled pieces were thermally sinterized (Nabetherm furnace, Germany) according to the manufacturer instructions. To simplify manufacturing, two peripheral slots were prepared with a dental diamond bur after milling and thermal processing.

Surface roughness measurements

The surface topography was characterized using both a white light interferometer (Xi 100 Ambios Technology) and a contact profilometer (XP-1, Ambios Technology). The entire inner surface of the zirconium sample was analyzed, and we obtained the same results regarding the roughness parameters, especially the amplitude parameters of arithmetical mean height [$S_a(\mu m)$] and root mean square height [$S_q(\mu m)$]. Results are presented as the mean ± standard deviation after 60 measurements.

Experimental design

This study was a preclinical animal study and conformed to the Interdisciplinary Principles and Guidelines for the Use of Animals in Research, Testing, and Education issued by the New York Academy of Sciences Adhoc Committee on Animal Research, Directive 2010/63/EU, national legislation (Law no.43/2014). The experimental protocol was approved by the Vasile Goldis Western University Ethics Committee.

A total of 30 adult male Wistar rats (200–250 g) were included. Before and during the experiment, the animals received a

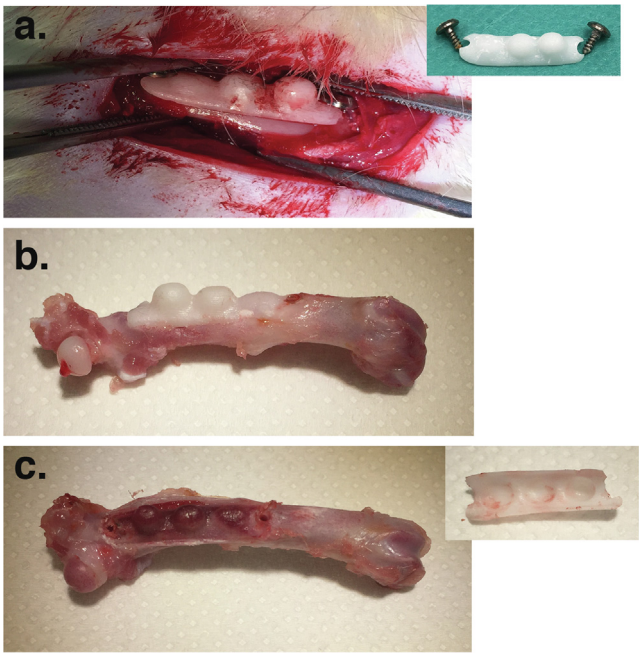

Fig. 2. Different steps of the surgical procedure. a. Placement of the zirconia membrane on the femur; b. Ex vivo femur post-surgery; c. Barrier removal highlighting three newly formed osseous domes on the femur.

standard diet and were housed in IVC cages with a 12-h light/dark cycle.

The surgical procedure was performed under ketamine/xylazine anesthesia. Three defects (corresponding to the center of each dome) were made in each femoral diaphysis using 2-mm-diameter trephine continuous irrigation with 0.9% NaCl. The customized CAD/CAM zirconia space-maintaining devices were secured in position by fixation screws (Fig. 2).

Throughout the experiment, the animals were clinically evaluated every day. The rats were euthanatized, and a retrieval procedure was performed at 2, 4, and 8 weeks (10 rats/time-point interval), based on our previous experience in bone regeneration research to capture the main key events of osteogenesis [26,27]. Femur tissues designated for histology and immunofluorescence were harvested and immersed in 4% paraformaldehyde (PFA) after acquiring gross and X-ray images.

High-resolution X-ray and bone mineral density measurements

The radiograph images of the sites were acquired by an in vivo imaging system (XTREME in-vivo Imaging Systems, Carestream, USA). For high-resolution X-ray imaging, the femurs were orientated along their long axis. Each GBR site in five animals/time point was measure for bone mineral density (BMD), and the mean values were recorded.

Histology and histomorphometrical analysis

Bone explants (n = 5/time point) were immersed for 5 days in a 4% paraformaldehyde fixing solution in PBS. Decalcification was performed over a 3-week period in Biodec R (Bio-Optics) at room temperature. Then, the samples were dehydrated in alcohols with increasing concentrations, clarified, and embedded in paraffin blocks. The samples were cut using a microtome (5 µm), and histological sections were subsequently stained with Gomori trichrome (Leica, Germany) for bone augmentation analysis.

The percentage area of the newly generated tissue (observed using a 4 × objective) was calculated relative to the area bound by the inner shape of each dome, which was taken to be 100%. The measurements were performed on five randomly selected fields/each dome under an optical microscope (Olympus BX43, Japan) using ImageJ software, as previously reported [27].

Osteogenesis and angiogenesis markers analysis

In vitro experiments

Pre-osteoblast cells from the MC3T3-E1 cell line (ATCC CRL-2593) were cultured in the recommended cell culture media supplemented with 10% fetal bovine serum (FBS, Life Technologies, Bleiswijk, Netherlands) and 1% antibiotics (Sigma-Aldrich, Darmstadt, Germany) under standard culture conditions (37 °C, humidity, and 5% CO_2). Preosteoblasts in the tenth passage were seeded on the surface of zirconia.

After 14 and 28 days of in vitro osteogenic differentiation, the resulting differentiated osteoblasts were fixed in PFA for 1 h and permeabilized with a 2% BSA/0.1% Triton X-100 solution at 4 °C and then incubated overnight at 4 °C with the primary antibodies of osteopontin and osteocalcin. Cell nuclei were stained with DAPI for 10 min.

In vivo experiments

Deparaffinization and rehydration of the decalcified femurs was performed. Antigen unmasking was performed using a sodium citrate buffer (pH 6.0) and blocked in 1% bovine serum albumin (BSA) and 5% normal goat serum in PBS for 1 h. Primary antibodies, i.e., rabbit polyclonal osterix antibody (Santa Cruz, sc-22536-R), rabbit polyclonal osteopontin antibody (Abcam, ab8448), rabbit polyclonal osteocalcin antibody (Santa Cruz, sc-30044), or PDGFRβ antibody (Abcam, ab32570), in a 1% BSA solution were added; then, the mixture was incubated overnight at 4 °C (1:100). The secondary antibody used was an Alexa Fluor dye conjugated (1:500) in an appropriate blocking solution for 1 h at room temperature in the dark, and nuclei were counterstained with DAPI.

The fluorescence intensity was measured in arbitrary units (a.u.) from 10 sections and analyzed by confocal microscopy (Leica TCS SP8 confocal microscope).

VEGFR2 protein expression was evaluated by immunohistochemistry using a Novolink Polymer Detection Systems Novocastra (RE7280-K, Leica Biosystems) according to the manufacturer's instructions. The sections were deparaffinized in Dewax solution (AR9222, Leica Biosystems) and rehydrated in alcohol solutions (100%, 95%, and 70%) and then exposed overnight to specific primary VEGFR2 antibody (dilution 1:200; ab2349). The Novolink polymer highlighted the protein VEGFR2 in the tissue.

Quantitative PCR (qPCR)

Murine preosteoblasts from the 3T3E1 cell line were seeded on the materials, and osteogenic differentiation was induced over 21 days. The total RNA was isolated from differentiated cells at 14 and 21 days by TRIzol (Thermo Fisher Scientific, Waltham, MA USA), and cDNA was obtained by reverse transcription using an iScript cDNA Synthesis kit (BioRad, Hercules, CA, USA). The gene expression of the osteogenic markers (*osteocalcin* and *osteopontin*) was evaluated by real-time PCR by SYBR Select MasterMix (Applied Biosystems, Vilnius, Lithuania) and Viia7 instruments. Normalization was performed against the glyceraldehyde 3-phosphate dehydrogenase (GAPDH) reference gene, and quantification was performed using the $2^{-\Delta\Delta Ct}$ method, according to MIQE guidelines. For gene expression studies, biological replicates were used (n = 3).

Statistical analysis

The achieved experimental data were analyzed using GraphPad Prism 3.03 software (GraphPad Software, Inc., La Jolla, CA, United States). For statistical analyses, the one-way ANOVA (and non-parametric) method was applied, followed by a Bonferroni correction post-test and comparison between all pairs of columns. A confidence interval of 95% was used. A statistically significant difference was considered for $p < 0.05$.

Results

Morphological aspects of the customized three-dome zirconia barrier

Customized CAD/CAM zirconia space-maintaining devices were 3D-sinterized with three domes of different heights [i.e., maximum (2.072 mm), medium (1.541 mm), and minimum (0.679 mm)] according to the rat femur 3D image obtained by optical scanning with an intraoral scanner (Fig. 1). All implanted three-dome zirconia-based bioceramic barriers had a similar design and a rough inner surface with $s_a = 2.53 \pm 0.061$ μm and $S_q = 23.63 \pm 0.089$ μm.

The photographs taken at 8 weeks (after removing the mold) show the formation of the three bone domes of increasing heights (Fig. 2).

Clinical evaluation

Post-operative clinical evaluation showed that there were no complications, and all rats survived the implantation period until the end of the experiment. All animals recovered their limb function within 24 h after surgery. The implanted site did not produce an inflammatory response, which showed the biocompatibility and non-toxicity of the barrier. Macroscopic images were taken before and after the implantation, which demonstrated the proper placement and stability of the customized zirconia barrier at the defect site.

High-resolution radiographic evaluation and BMD analysis

The mineralization of new bone was evident at week 4 and extended from the edges of the domes to the center. The radiopacity in the middle of the sites was low; low mineralization was observed in some peripheral areas of the maximum- and medium-height domes. Ossification was advanced at 8 weeks for all three domes owing to mineral deposition and ingrowth of new bone (Fig. 3). The BMD analysis showed considerable bone healing at 8 weeks for all three GBR sites compared with that at week 4 ($p < 0.001$). The best results were obtained for the minimum height compared to those for the medium and maximum heights of GBR sites induced by the zirconia space-maintaining devices. The BMD result obtained from the control femoral diaphysis of approximately 1.6 g/cm^3 is similar to previously published results [20]. Therefore, we can assume that at week 8, the newly formed bone had a mineral density of approximately 31.8% of a mature femoral bone.

Histology and histomorphometrical analysis

Gomori's trichrome was used to highlight the bone tissue in the GBR sites. Representative Gomori's trichrome panoramic images corresponding to all three time points are shown in Fig. 4A.

After 2 weeks, most GBR sites were invaded with connective tissue elements and osteoprogenitor cells originating from bone marrow (Fig. 4B1). The formation of ossification centers and active osteoblasts in addition to remnant blood clot fragments was observed (Fig. 4B1).

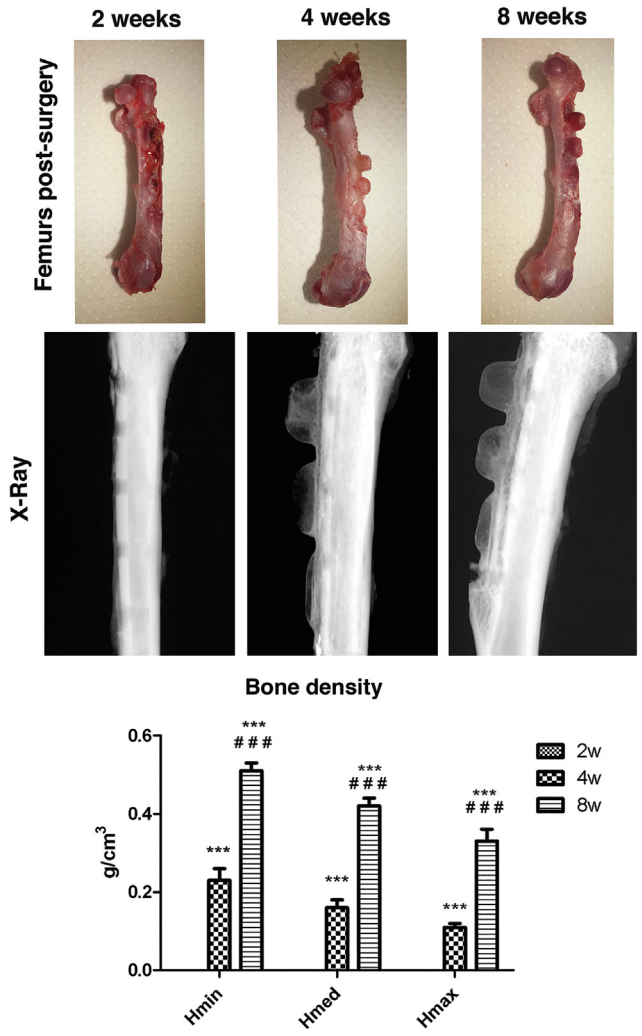

Fig. 3. Representative photographs post-surgery. X-ray micrographs and bone density analysis of the rat femoral GBR sites at 2, 4, and 8 weeks. ***p < 0.001 compared to week 2; ###p < 0.001 compared to week 4.

After 4 weeks, a new trabecular bone with active osteoblasts at the edges was observed (Fig. 4B2). Bone formation starts from the periphery of the barrier and progresses to the center. A layer of osteoblasts marked the limit of the newly formed tissue, which showed an active osteogenesis process. Nevertheless, immature bone areas and a rather wide central and peripheral fibroconnective soft tissue were still evident, particularly for medium and maximum height space-maintaining domes (Fig. 4A).

More of the osteoid matrix was observed 8 weeks post-implantation compared with that at week 4 (Fig. 4A). The presence of connective tissue lining between the barrier and new osseous tissue was not observed (Fig. 4A). However, several trabecula of newly formed bone tissues were observed in many parts of the slides and were segregated by bone marrow (Fig. 4B3). Of note, the tissue almost showed a transition from immature to mature bone tissue after 8 weeks. In addition, the formation of a Haversian system in the newly formed bone was observed (Fig. 4B3).

The histomorphometrical analysis showed that the zirconia-based minimum height dome had a significantly higher percent of new tissue (70% ± 5.50) compared to the medium-height (47.40% ± 4.51) and maximum-height (34.40% ± 4.16) zirconia domes and was significantly time-dependent for the medium and maximum sizes (more than 1.5-mm high) (Table 2).

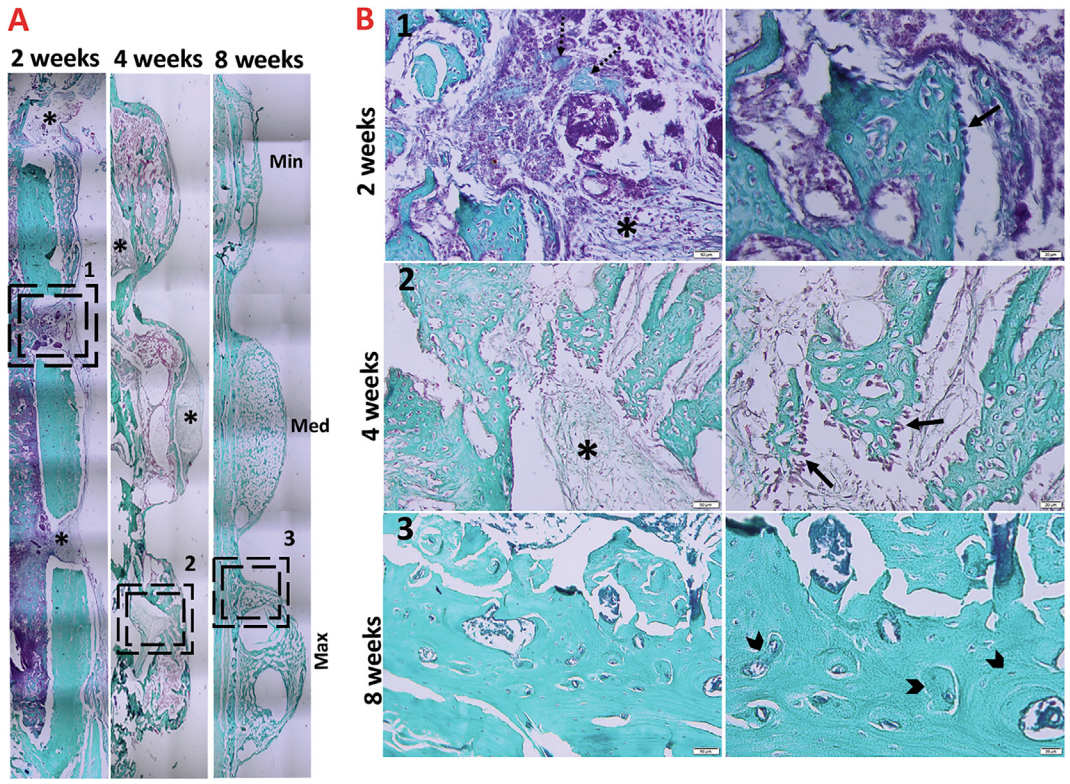

Fig. 4. Photomicrographs (Gomori's trichrome) of the GBR sites. A. Panoramic view (200 μm) of the rat femoral GBR sites at 2, 4, and 8 weeks; **B.** Histological details (50 μm) of the representative events of osteogenesis on GBR sites at week 2 (1), week 4 (2), and week 8 (3); fibro-connective tissue (*), small bone islands (dotted arrow), osteoblasts (arrow), and osteons (arrowhead).

Osteogenic differentiation analysis

Murine preosteoblasts seeded on zirconia showed an increasing profile for OPN and PCN, which was detected after up to 28 days of in vivo differentiation under pro-osteogenic conditions by qPCR; a similar pattern was observed by immunofluorescence (Fig. 5A).

Assays of osterix (OSX), osteopontin (OPN), and osteocalcin (OCN) by immunofluorescence were conducted to determine the expression of osteoblast-related markers during osteogenesis in vivo (Fig. 5B). Immunofluorescence-targeting OSX was observed as early as 2 weeks and became significant starting at week 4 ($p < 0.001$), which was associated with osteoblastic activities (Fig. 5Bb). OPN had a stronger expression than OCN, and both were significantly higher by week 8 compared to those by week 2 ($p < 0.001$) (Fig. 5Bb).

Angiogenesis progression analysis

The immunofluorescence analysis of PDGFRβ (Fig. 5C) showed that the new tissue area formed under the zirconia barrier exhibited a gradual increase in the expression level from week 2 to week 4 post-implantation ($p < 0.05$) and remained at high levels until week 8. (Fig. 5Cb). The immunohistochemical expression of VEGFR2 followed the same pattern (Fig. 5D).

Table 2
Percentage area of newly generated tissue under the domes at weeks 4 and 8.

Newly generated tissue/total dome area %	Minimum height dome Mean ± SD	Medium height dome Mean ± SD	Maximum height dome Mean ± SD
4 weeks	60.80 ± 7.53	30.80 ± 2.77	19.40 ± 2.70
8 weeks	70.20 ± 5.50	47.40 ± 4.51***	34.40 ± 4.16***

*** $p < 0.001$ compared to week 4.

Discussion

The guidance of bone cells to an area that has been previously devoid of bone tissue (to generate new bone and increase bone volume) is essential for bone tissue engineering. Therefore, guided bone regeneration (GBR) can be provided with barriers; these structures should possess properties that allow osteoprogenitor cells to migrate and, at the same time, act as a barrier for the migration of soft cells, which can disrupt osteoconductive activity [20]. Maintaining a stable barrier position is important to ensure GBR, whereas partial or total collapse will lead to bone failure or to a smaller volume of bone tissue [28]. This clinical application is mainly used in dentistry but can also serve as a critical bone addition for orthopedics [7,15].

Based on these results, we aimed to assess GBR using a new experimental model of a customized 3D CAD/CAM zirconia barrier. This barrier was designed to ensure proper barrier stability and complete isolation, which allows sufficient vertical and horizontal bone augmentation at the chosen site. The barrier was designed with three domes of increasing heights to evaluate the conditions leading to the highest amount of new bone formation and to investigate the related time-dependent molecular events of osteogenesis influenced by the barrier. The maximum height was set at 2 mm, which is the threshold for the vertical bone defect, as defined in dentistry [29]. Certainly, a positive screening with this barrier model will require evaluation of the vertical addition of bone to alveolar bone, and some variables, such as age, sex, and smoking, can then change the response in clinical applications. In orthopedics, the model can be applied directly for bone reconstruction assessment.

Post-surgical clinical examination demonstrated the absence of inflammatory signs (as a foreign body reaction at evaluated time points), which showed the biocompatibility of the zirconia

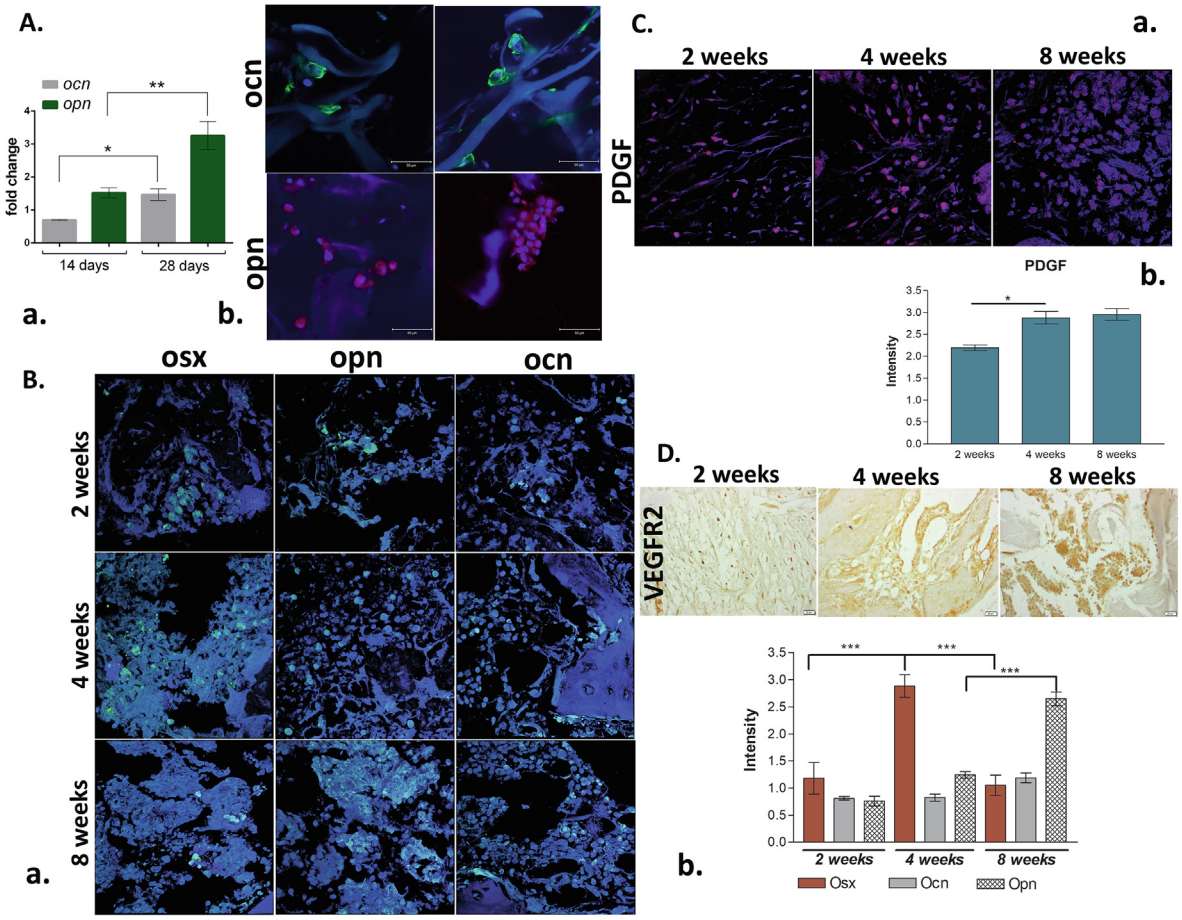

Fig. 5. Evaluation of osteogenesis and angiogenesis markers. A. *Osteogenesis markers in 3T3E1 cells after* in vitro *differentiation under pro-osteogenic conditions on the zirconia surface (positive control).* **a.** OCN and OPN profiles of gene expression at 14 and 28 days; *p < 0.05; **p < 0.01. The fold change in the qPCR data analysis was determined by the $2-\Delta\Delta Ct$ method. **b.** Protein expression of osteogenic specific markers OCN and OPN at 14 and 28 days by confocal microscopy. The nuclei are labeled in blue for DAPI, in green for OCN, and in red for OPN; **B.** *Osteogenesis markers in GBR sites.* **a.** OSX, OPN, and OCN protein expression as revealed by confocal microscopy at 2, 4, and 8 weeks. OSX/OCN/OPN are labeled in green, and the nuclei are counterstained with DAPI in blue; **b.** Fluorescence intensities of the green signal were quantified in at least 10 random fields in each dome from three independent specimens; the data are expressed as fold changes of relative fluorescence units at 2, 4, and 8 weeks. ***p < 0.001 compared to weeks 2 and 4; **C.** *Angiogenesis markers in GBR sites.* **a.** PDGFRβ protein expression as revealed by confocal microscopy at 2, 4, and 8 weeks. PDGFRβ is labeled in red, and the nuclei are counterstained with DAPI. **b.** The fluorescence intensities of the red signal were quantified in at least 10 random fields in each dome from three independent specimens; the data are expressed as fold changes of relative fluorescence units at weeks 2, 4, and 8. *p < 0.05 compared to week 2. D. Immunohistochemical stain of VEGFR2 at 2, 4, and 8 weeks.

barrier. Previous studies have shown the biocompatibility of zirconia-based bioceramics, which agrees with our observations [30]. Experimental studies on animal models have shown good biocompatibility of zirconia implants, which is characterized by the high adhesion rates of newly formed bone to the material [31,32].

Furthermore, the microscopic analysis of newly formed bone tissue showed no adverse reactions and no inflammatory signs. Bone resorption was not observed, which is common in bone graft treatments. Thus, the barrier designed by us offers high stability and is a perfect fit for the implant site, which are the most important factors promoting bone osteogenesis. The results show that our surgical model and fully isolated GBR sites by zirconia domes guarantee that enough osteoprogenitor cells originated from bone marrow to fill the domes during the first 2 weeks. During the next 2 weeks, forming bone cells migrated to the inner surface of zirconia domes, depending on the height and time interval. This observation confirms the bone conductivity of the stable zirconia barrier for cells that populate and differentiate to bone inside the domes, as suggested by radiographic evaluation and verified by macroscopic gross evidence. Meanwhile, the surface roughness of the zirconia barrier suggested a possible positive impact on the satisfactory vertical and horizontal bone tissue production and on faster kinetics, which is supported by other studies [33,34]. Moreover, Anderud et al. [19] speculated that surface topography was more important in guided bone augmentation than the surface chemistry.

Histomorphometry revealed that bone formation started to develop by osteoblastic proliferation as early as after 4 weeks, starting with the inner surface of the dome cavity (Fig. 4A and 4B2). Healing continued by filling the entire dome volume; filling was more significant at week 8 (Fig. 4A and 4B3), compared to that at week 4 ($p < 0.001$). The bone volume below the zirconia barrier was better protected with reduced relative displacement that may disturb bone formation. The maximum height of 1.7 mm was reached by week 8; the domes were filled with osteoid areas, mineralized bone tissue, marrow spaces, and tissue already undergoing osteogenesis. The effect of bone augmentation with individualized ceramic sheets has been previously studied by Malmstrom et al. [20] in a pilot study. Specifically, bone was regenerated in the entire inner volume of all ceramic sheets in 7 months, gaining 1.67 mm of bone volume in the vertical dimension for patient 1 and 3.88 mm and 3.15 mm for patients 2 and 3, respectively. In another study, zirconia scaffolds inserted in bone defects in the mandible of a dog model reached 21% of new bone volume in

6 weeks and 33% for hydroxyapatite (HA) enriched zirconia scaffolds [21]. In our study, the customized zirconia barrier allowed new bone formation and osteoconduction within the space created in both vertical and horizontal directions with a good biological acceptance of the material. The amount of obtained bone in the spaces with three different heights was limited by vertical bone regeneration; specifically, the dynamics of vertical growth of the tissues decreased with an increased in the dome height.

The growth was faster for the small dome with no significant differences observed at week 8 compared to week 4. However, there was a statistically significant difference between 4- and 8-week specimens in the amount of newly generated tissue under medium and high dome heights ($p < 0.001$).

Moreover, we investigated the osteogenic differentiation potential of customized CAD/CAM zirconia membranes as a function of dome heights. During GBR, the early osteogenesis process was quickly activated for the sites flooded with bone marrow; OSX positive staining was observed starting at week 2. This is important because osterix is a transcription factor that is expressed once mesenchymal cells have differentiated into preosteoblasts, which is essential for osteogenesis and bone formation [35]. Furthermore, OSX and RUNX2 activate sclerostin gene expression [36] and stimulate protein synthesis by osteocytes in a mineralized matrix [37].

Meanwhile, osteoblast differentiation was also stimulated by the zirconia barrier during late osteogenesis, as shown by the immunopositivity of both OPN and OCN at week 4 and overexpression at week 8. The significantly higher expression of OPN during this time interval produced embedded osteoblasts within the osteoid areas relatively soon after the initial matrix formation, which continued throughout the maturation of the newly formed bone and spread to the entire dome area [38]. OCN is a protein responsible for calcium ion binding; it envelopes mature osteoblasts in a mineralized matrix, which transform into osteocytes, and retains its expression. Thus, OCN, which is considered a late marker of osteogenesis appeared to be fluorescence labelled only in the area of mineralized bone [39], which was less expressed overall than OPN at week 8.

Angiogenesis is essential for the regeneration of large areas of bone defects. The integrity of the vascular network is important for providing oxygen and nutrients to bone tissue; thus, angiogenesis should increase osteogenesis [40]. PDGF is a growth factor that is essential for bone regeneration through stimulation of angiogenesis, and it promotes other osteogenic pathways [41]. PDGF is a chemotactic and mitogenic factor for osteoblasts; it directly or indirectly promotes angiogenesis by VEGF upregulation [42]. Osteoblast expression is independently regulated by PDGF receptors (PDGFRs) [43]. Moreover, it has been shown that deletions of VEGF receptor 2 in osteoblastic cells showed low bone density and decreased number of osteoprogenitors in bone marrow [44], and specifically, deletion of VEGF in osteoblasts disrupts the coupling of angiogenesis and osteogenesis and delays the healing process [45]. Thus, in our study, the increased expression of PDGFR and VEGFR2 may also explain the considerably enriched bone formation in GBR sites, which facilitates coupling between vasculogenesis and osteogenesis during bone regeneration [46,47].

Conclusions

The use of a customized milled zirconia-based bioceramic barrier provides useful information on progressive bone tissue formation, depending on the volume of isolated space created for GBR and on molecular events leading to satisfactory vertical and horizontal bone augmentation and osteointegration.

To conclude, the proposed customized three dome space-maintaining barrier is suitable as an experimental tool to assess the potential of using designed barriers in dentistry and orthopedics to promote new bone formation and to determine their space- and time-dependent limitations. Meanwhile, guided bone augmentation for dentistry requires subsequent evaluation on an alveolar bone model, followed by clinical implementation.

Author contributions

A. Petre and A. Hermenean contributed to the conception, design, data acquisition, analysis, and interpretation; they drafted and critically revised the manuscript. C. Balta, H. Herman, and S. Gharbia contributed to the data acquisition and analysis; they drafted the manuscript. A. Codreanu, B. Onita, N. Anghel, S. Drafta, and A.G. Hermenean contributed to the data acquisition and drafting of the manuscript. S.R. Ignat and S. Dinescu performed the in vitro murine preosteoblasts osteogenic differentiation. I. Urzica performed the zirconia surface roughness measurements. L. Oancea contributed to the interpretation, drafting, and critical revision of the manuscript. All authors gave final approval and agreed to be accountable for all aspects of the work.

Funding

No **funding** to declare

Compliance with Ethics Requirements

All Institutional and National Guidelines for the care and use of animals (fisheries) were followed:

This study is a preclinical animal study and conformed to the Interdisciplinary Principles and Guidelines for the Use of Animals in Research, Testing, and Education issued by the New York Academy of Sciences Adhoc Committee on Animal Research, Directive 2010/63/EU, national legislation (Law no. 43/2014). The experimental protocol was approved by the Vasile Goldis Western University Ethics Committee.

Declaration of Competing Interest

The authors declare that the research was conducted in the absence of any commercial or financial relationships that could be construed as a potential conflict of interest.

References

[1] Schropp L, Wenzel A, Kostopoulos L, Karring T. Bone healing and soft tissue contour changes following single-tooth extraction: a clinical and radiographic 12-month prospective study. Int J Periodontics Restorative Dent 2003;23(4):313–23.
[2] Liu J, Kerns DG. Mechanisms of guided bone regeneration: a review. Open Dent J 2014;8:56–65.
[3] Van der Weijden F, Dell'Acqua F, Slot DE. Alveolar bone dimensional changes of post-extraction sockets in humans: a systematic review. J Clin Periodontol 2009;36(12):1048–58.
[4] Tallgren A. The continuing reduction of the residual alveolar ridges in complete denture wearers: a mixed-longitudinal study covering 25 y. 1972. J Prosthet Dent 2003;89(5):427–35.
[5] Bernstein S, Cooke J, Fotek P, Wang HL. Vertical bone augmentation: where are we now?. Implant Dent 2006;15(3):219–28.
[6] Sheikh Z, Sima C, Glogauer M. Bone replacement materials and techniques used for achieving vertical alveolar bone augmentation. Materials 2015;8(6):2953–93.
[7] Dimitriou R, Mataliotakis GI, Calori HM, Giannoudis PV. The role of barrier membranes for guided bone regeneration and restoration of large bone defects: current experimental and clinical evidence. BMC Medicine 2012;10:81.
[8] Rakhmatia YD, Ayukawa Y, Furuhashi A, Koyano K. Current barrier membranes: titanium mesh and other membranes for guided bone regeneration in dental applications. J Prosthodont Res 2013;57(1):3–14.
[9] Retzepi M, Donos N. Guided Bone Regeneration: biological principle and therapeutic applications. Clin Oral Implants Res 2010;21(6):567–76.

[10] Behring J, Junker R, Walboomers XF, Chessnut B, Jansen JA. Toward guided tissue and bone regeneration: morphology, attachment, proliferation, and migration of cells cultured on collagen barrier membranes. A systematic review. *Odontology* 2008;96:1–11.
[11] Hammerle C, Jung R. Bone augmentation by means of barrier membranes. Periodontology 2000;33(2003):36–53.
[12] Meinig RP. Clinical use of resorbable polymeric membranes in the treatment of bone defects. Orthop Clin North Am 2010;41:39–47.
[13] von Arx T, Broggini N, Jensen SS, Bornstein MM, Schenk RK, Buser D. Membrane durability and tissue response of different bioresorbable barrier membranes: a histologic study in the rabbit calvarium. Int J Oral Maxillofac Implants 2005;20:843–53.
[14] McAllister BS, Haghighat K. Bone augmentation techniques. J Periodontol 2007;78:377–96.
[15] Elgali I, Omar O, Dahlin C, Thomsen P. Guided bone regeneration: materials and biological mechanisms revisited. Eur J Oral Sci 2017;201:1–23.
[16] Mangano F, Zecca P, Pozzi-Taubert S, Macchi A, Ricci M, Luongo G, et al. Maxillary sinus augmentation using computer-aided design/computer-aided manufacturing (CAD/CAM) technology. Int J Med Robot 2013;9 (3):331–8.
[17] Yen HH, Stathopoulou PG. CAD/CAM and 3D-printing applications for alveolar ridge augmentation. Curr Oral Health Rep 2018;5(2):127–32.
[18] Ciocca L, Lizio G, Baldissara P, Sambuco A, Scotti R, Corinaldesi G. Prosthetically CAD-CAM-guided bone augmentation of atrophic jaws using customized titanium mesh: preliminary results of an open prospective study. J Oral Implantol 2018;44(2):131–7.
[19] Anderud J, Abrahamsson P, Jimbo R, Isaksson S, Adolfsson E, Malmström J, et al. Guided bone augmentation using ceramic space-maintaining devices: the impact of chemistry. Clin, Cosmetic Invest Dentistry 2015;7:45–53.
[20] Malmström J, Anderud J, Abrahamsson P, Wälivaara D, Isaksson SG, Adolfsson E. Guided bone regeneration using individualized ceramic sheets. Int J Oral Maxillofac Surg 2016;45(10):1246–52.
[21] Aboushelib MN, Shawky R. Osteogenesis ability of CAD/CAM porous zirconia scaffolds enriched with nano-hydroxyapatite particles. Int J Implant Dent 2017;3(1):21.
[22] Caiazza S, Colangelo P, Bedini R, Formisano G, De Angelis G, Barrucci S. Evaluation of guided bone regeneration in rabbit femur using collagen membranes. Implant Dentistry 2000;9(3):219–25.
[23] Binsalah MA, Ramalingam S, Alkindi M, Nooh N, Al-Hezaimi K. Guided bone regeneration of femoral segmental defects using equine bone graft: an in-vivo micro-computed tomographic study in rats. J Invest Surg 2018;32(5):456–546.
[24] Ender A, Zimmermann M, Mehl A. Accuracy of complete- and partial-arch impressions of actual intraoral scanning systems in vitro. Int J Comput Dent 2019;22(1):11–9.
[25] Abduo J, Elseyoufi M. Accuracy of intraoral scanners: a systematic review of influencing factors. Eur J Prosthodont Restor Dent 2018;26:101–21.
[26] Hermenean A, Codreanu A, Herman H, Rosu M, Mihali CV, Ivan A, et al. Chitosan-graphene oxide 3D scaffolds as promising tools for bone regeneration in critical-size mouse calvarial defects. Sci Rep 2017;7(1):16641.
[27] Dinescu S, Ionita M, Ignat SR, Costache M, Hermenean A. Graphene oxide enhances chitosan-based 3D scaffold properties for bone tissue engineering. Int J Mol Sci 2019;20:5077.
[28] Dupoirieux L, Pourquier D, Picot MC, Neves M. Comparative study of three different membranes for guided bone regeneration of rat cranial defects. Int J Oral Maxillofac Surg 2001;30(1):58–62.
[29] Cucchi A, Ghensi P. Vertical guided bone regeneration using titanium-reinforced d-PTFE membrane and prehydrated corticocancellous bone graft. Open Dent J 2014;8:194–200.
[30] Marques G, Marques Padovan LE, Matsumoto MA, Domingos Ribeiro Júnior P, Mattias Sartori E, Claudino M. Bone healing in titanium and zirconia implants surface: a pilot study on the rabbit tibia. RSBO Revista Sul-Brasileira de Odontologia 2013;10(2):110–115.
[31] Sennerby L, Dasmah A, Larsson B, Iverhed M. Bone tissue responses to surface-modified zirconia implants: A histomorphometric and removal torque study in the rabbit. Clin Implant Dent Relat Res 2005;7(Suppl 1):S13–20.
[32] Akagawa Y, Hosokawa R, Sato Y, Kamayama K. Comparison between freestanding and tooth-connected partially stabilized zirconia implants after two y' function in monkeys: a clinical and histologic study. J Prosthet Dent 1998;80(5):551–8.
[33] Wennerberg A, Alberktsson T. On implant surfaces: a review of current knowledge and opinions. Int J *Oral Maxillofac Implants* 2010;25(1):63–74.
[34] Wennerberg A, Albrektsson T. Effects of titanium surface topography on bone integration: a systematic review. Clin Oral Implants Res 2009;20(4):172–84.
[35] Nakashima K, Zhou X, Kunkel G, Zhang Z, Deng JM, Behringer RR, et al. The novel zinc finger-containing transcription factor osterix is required for osteoblast differentiation and bone formation. Cell 2002;108(1):17–29.
[36] Pérez-Campo FM, Santurtún A, García-Ibarbia C, Pascual MA, Valero C, Garcés C, et al. Osterix and RUNX2 are transcriptional regulators of sclerostin in human bone. Calcif Tissue Int 2016;99(3):302–9.
[37] van Bezooijen RL, Bronckers AL, Gortzak RA, Hogendoorn PC, van der Wee-Pals L, Balemans W, et al. Sclerostin in mineralized matrices and van Buchem disease. J Dent Res 2009;88(6):569–74.
[38] Morinobu M, Ishijama M, Rittling SR, Tsuji K, Yamamoto H, Nifuji A, et al. Osteopontin expression in osteoblasts and osteocytes during bone formation under mechanical stress in the calvarial suture in vivo. J Bone Miner Res 2003;18(9):1706–15.
[39] Kandiah K, Muthusamy P, Mohan S, Venkatachalam R. TiO2-graphene nanocomposites for enhanced osteocalcin induction. Mater Sci Eng C Mater Biol Appl 2014;38:252–62.
[40] Lin Y, Xiao W, Bal BS, Rahaman MN. Effect of copper-doped silicate 13–93 bioactive glass scaffolds on the response of MC3T3-E1 cells in vitro and on bone regeneration and angiogenesis in rat calvarial defects in vivo. Mater Sci Eng C Mater Biol Appl 2016;67:440–52.
[41] Hankenson KD, Dishowitz M, Gray C, Schenker M. Angiogenesis in bone regeneration. Injury 2011;42(6):556–61.
[42] Hollinger JO, Hart CE, Hirsch SN, Lynch S, Friedlaender GE. Recombinant human platelet-derived growth factor: biology and clinical applications. J Bone Joint Surg Am 2008;90(Suppl 1):48–54.
[43] Shah P, Keppler L, Rutkowski J. A review of platelet derived growth factor playing pivotal role in bone regeneration. J Oral Implantol 2014;40(3):330–40.
[44] Liu Y, Berendsen AD, Jia S, Lotinun S, Baron R, Ferrara N, et al. Intracellular VEGF regulates the balance between osteoblast and adipocyte differentiation. J Clin Invest 2012;122:3101–13.
[45] Hu K, Olsen BR. Osteoblast-derived VEGF regulates osteoblast differentiation and bone formation during bone repair. J Clin Invest 2016a;126:509–526.
[46] Caplan AI, Correa D. PDGF in bone formation and regeneration: new insights into a novel mechanism involving MSCs. J Orthop Res 2011;29(12):1795–803.
[47] Grosso A, Burger MG, Lunger A, Schaefer DJ, Banfi A, Di Maggio N. It takes two to tango: coupling of angiogenesis and osteogenesis for bone regeneration. Front Bioeng Biotechnol 2017;5:68.